How to cite: *Angew. Chem. Int. Ed.* **2023**, *62*, e202315143
doi.org/10.1002/anie.202315143

COF Films Hot Paper

Adjustable Plane Curvature of Covalent Organic Framework Enabling Outstanding Dielectric, Electret, and High-Temperature Processing Properties

Donglin Chen, Jinpeng Li, Xudong Mei, Xiaoyun Liu, Peiyuan Zuo, Xunlin Qiu, and Qixin Zhuang**

Abstract: With the rapid development of integrated circuits towards miniaturization and complexity, there is an urgent need for materials with low dielectric constant/loss and high processing temperatures to effectively prevent signal delay and crosstalk. With high porosity, thermal stability, and easy structural modulation, covalent organic frameworks have great potential in the field of low dielectric materials. However, the optimization of dielectric properties by modulating the conjugated/plane curvature structure of covalent organic frameworks (COFs) has rarely been reported. Accordingly, we herein innovatively prepare COF films with adjustable planar curvature, hence possessing ultralow dielectric constant (1.9 at 1 kHz), ultralow dielectric loss at 1 kHz (0.0029 at room temperature, 0.0052 at 200 °C), high thermal decomposition temperature (5 % weight loss temperature, 473 °C) and good hydrophobicity (water contact angle, 105.3°). Also, to the best of our knowledge, we are the first to report that the resulting COF film enables high surface potential (≈320 V) for one week, attributing to its intrinsic high porosity, thus presenting great potential in electret applications. Accordingly, this innovative work provides a readily available and scalable idea to prepare materials with comprehensively excellent dielectric and electret properties as well as high processing temperatures simultaneously for advanced electronic device applications.

Introduction

With the ever-increasing demand for semiconductors and the 5G communication industry, integrated circuits have begun to develop towards high complexity and miniaturization.[1] Currently, advanced chips usually integrate billions of transistors with an average size of metal interconnects downscaling to 10 nm.[2] However, this evolution inevitably brings problems such as resistance-capacitance (RC) delay, crosstalk, and power loss.[3] To meet the urgent requirements for interlayer media of packaging materials and printed circuit board materials, many high-performance polymers have been developed, such as polyimide,[4] polybenzoxazine,[5] benzoxazole,[6] epoxy resin,[7] maleimide,[8] all of them are developed to yield ultralow dielectric constant (k) materials ($k < 2.5$) to thus replace the traditional silicon dioxide ($k \approx 4$).

Different from traditional polymer based dielectrics, covalent organic framework (COF) features a typically periodic network structure, thus endowing the COF films with intrinsic high porosity, high crystallinity, excellent optoelectronic performance, and good thermal stability as well as low density concurrently.[9] In the past two decades, COF has been widely studied and applied to gas separation,[10] energy storage,[11] catalysis,[12] sensing,[13] semiconductor with high charge mobility, and other advanced field.[14] However, the research of COF in electronic devices, especially in dielectric and electrets, is still in its infancy. COF with adjustable pore size, high crystallinity, high specific surface area, and porosity, could be an ideal candidate for a novel low-k material compared to traditional polymers. Moreover, the cross-linked structure of COF endows itself with intrinsic low dielectric loss and thermal expansion coefficient. Wang et al.[15] synthesized COFs with different branch chain lengths through the method of interface synthesis, furthering conducting a preliminary study on the dielectric properties of COFs. However, due to the introduction of long alkyl branch chains, the friction between the long branch chains is increased during the orientation process, thus inevitably giving rise to serious dielectric loss. Evans et al.[16] synthesized high-quality COF film by template colloid method. The COF film features an ultra-low dielectric constant and high thermal conductivity, which greatly inspired the further development of COF in the low dielectric field. However, due to the characteristic of easy hydrolysis of borate ester COF,[9c,17] the borate ester-derived COF can hardly be well used in a wet environment, which seriously limits its dielectric applications. Accordingly, we still face great challenges in terms of precious synthesis

[*] D. Chen, J. Li, X. Liu, P. Zuo, Q. Zhuang
Key Laboratory of Advanced Polymer Materials of Shanghai, School of Materials Science and Engineering, East China University of Science and Technology
Shanghai 200237 (P. R. China)
E-mail: pyzuo@ecust.edu.cn
qxzhuang@ecust.edu.cn
X. Mei, X. Qiu
School of Mechanical and Power Engineering,
East China University of Science and Technology
Shanghai 200237 (P. R. China)

for COF films with comprehensively excellent properties such as low dielectric constant, low dielectric loss, hydrophobicity, high thermal stability as well as thermal conductivity. Moreover. The COF with large porosity and specific surface area could act as charge trapping sites to store charges to further apply as electrets, which show great potential to be used in electrostatic adsorption, filtration, and electret nanogenerators.[18] Unfortunately, to our knowledge, there rarely exist any relevant studies for COF in electret applications. As such, it seems extremely urgent and essential to focus on this inspiring research topic.

In our study, inspired by crawling caterpillars, we mainly aim to reduce interlayer electron coupling of COF plane periodic structure using methylene flexible groups. We adopted a simple method to synthesize a series of COF or covalent organic polymers (COP) with different surface bending degrees and systematically studied the effects of different bending degrees on the crystallinity, dielectric properties, thermal stability, and charge storage capacity of the products. These COF or COP (denoted as TFB-BZD_X-MDA_{3-X}-COF or COP film, X=0,1,2,3) are prepared by covalently linking 4,4′-diamino biphenyl (BZD), 4,4′-diamino-diphenylmethane (MDA) and 1,3,5-Benzenetricarboxaldehyde (TFB) in different proportions through interfacial polymerization (Figure 1). The prepared COF or COP thin films exhibit low dielectric constant/loss and acceptable charge storage capacity while maintaining high thermal stability and outstanding hydrophobic properties. Noticeably, the TFB-BZD_2-MDA_1-COF possesses good dielectric properties, thermal stability, and a low thermal expansion coefficient concurrently. The detailed dielectric constant reaches as low as 1.9 while the dielectric loss is only 0.0029 at room temperature and 0.0052 at 200 °C. Meanwhile, the thermal decomposition temperature is up to 473 °C and the thermal expansion coefficient is 44 ppm/k. On the other hand, the TFB-BZD_1-MDA_2-COF shows the best charge storage capacity, maintaining a surface potential of about 320 V after a week of storage under ambient conditions. These excellent characteristics of the as-prepared COF films enable us to have an insightful view to evaluate the periodic two-dimensional network structured COF application potentials in terms of typical low-k materials for smart electronic circuit devices.

Results and Discussion

In this work, we prepared COF films with different planar curvatures by adjusting the BZD and MDA ratios during interfacial polymerization at room temperature. The methylene provided by MDA not only served a role in increasing the degree of planar curvature[19] but also improved the hydrophobicity of the COF films, making them more suitable for applications in humid environments.[3b]

By density functional theory (DFT) calculations for BZD and MDA, we found that the nitrogen atoms of BZD and MDA have the same charge density (−0.834), so we can assume that BZD and MDA have similar nucleophilic ability, as such resulting in similar reactivity (Figure S1).

We verified the crystal structure of TFB-BZD_X-MDA_{3-X}-COF through powder X-ray diffraction (PXRD) and deduced it through theoretical simulation. the force field of

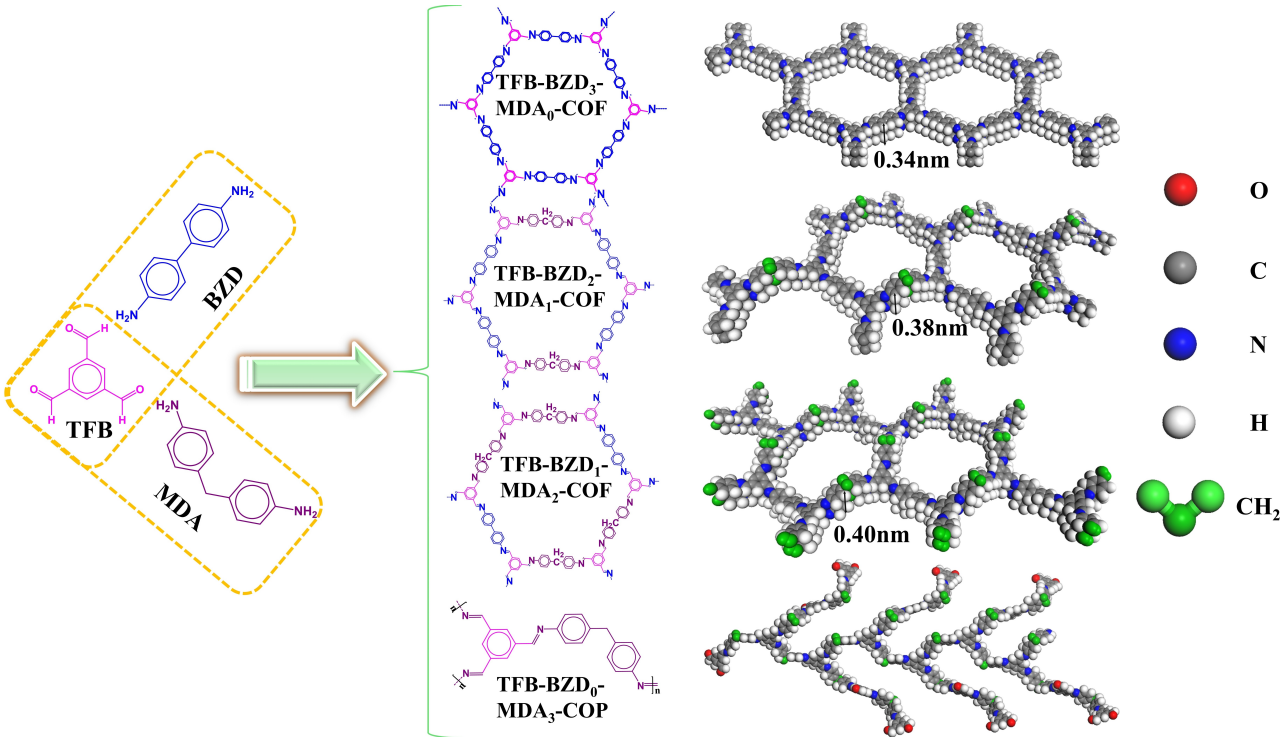

Figure 1. Structural drawing of TFB-BZD_3-MDA_0-COF, TFB-BZD_2-MDA_1-COF, TFB-BZD_1-MDA_2-COF and TFB-BZD_0-MDA_3-COP.

TFB-BZD_3-MDA_0-COF, TFB-BZD_2-MDA_1-COF, and TFB-BZD_1-MDA_2-COF were optimized to obtain their symmetry characteristics. The space group of TFB-BZD_3-MDA_0-COF is P6/M, while the types for TFB-BZD_2-MDA_1-COF and TFB-BZD_1-MDA_2-COF are P2. The experimental data is consistent with the PXRD of the AA stacking model (Figure S2a and Figure S2b).

The films of TFB-BZD_3-MDA_0-COF and TFB-BZD_2-MDA_1-COF show good crystallinity according to the PXRD patterns in Figure 2b. The diffraction peaks of TFB-BZD_3-MDA_0-COF at 3.58, 6.16, and 7.02° correspond to (100), (110), and (200) facets, respectively. The diffraction peaks of TFB-BZD_2-MDA_1-COF at 3.58, 6.24, and 7.02° correspond to the (100), (20−1), and (20−2) facet, respectively. The diffraction peak of TFB-BZD_1-MDA_2-COF at 3.62° corresponds to the (001) crystal plane, they have similar peak positions in the PXRD pattern, which is because they have similar hexagonal pores and pore sizes. TFB-BZD_0-MDA_3-COP shows no crystal diffraction peak. All COF films show a broader diffraction with the increase of MDA content. This is because the addition of MDA with flexible methylene structures enhances the degree of planar bending and interlayer distance of COF (Figure 1), thus leading to the weakening of π-stacking between benzene rings and enabling the decreased crystallinity of COF.

We also characterized the chemical components of TFB-BZD_X-MDA_{3-X}-COF or COP. All films exhibit typical C=N peaks at 1621 cm^{-1} (Figure 2a). The -NH_2 bimodal peaks of BZD and MDA at 3388 cm^{-1} and 3430 cm^{-1} disappear, while the intensity of the C=O peak of TFB significantly decreases at 1700 cm^{-1}.[12c] This indicates that aldehydes and amines have successfully carried out the Schiff base reaction.[20] The C=O peak still exists in the TFB-BZD_X-MDA_{3-X}-COF or COP infrared spectrum, which is mainly attributed to the terminal aldehyde group at the edge of COF or COP.[9b] In the ^{13}C cross-polarization/magic-angle spinning (CP-MAS) solid-state NMR spectra, the peaks at 157[21] and 41 ppm correspond to the carbon on the imine and the carbon on the MDA methylene, respectively (Figure S3a–d). This also indicates the success of the Schiff base reaction and the accurate synthesis of MDA-derived COF.

To further illustrate the difference between the four films versus the content of MDA, the X-ray photoelectron spectroscopy (XPS) test was performed to calculate the peak area ratios of C=C double bonds and C–C single bonds. As shown in Figure S4a–d, the C 1s spectra for films can be deconvoluted to five peaks centered at around 283.1, 284.0, 284.8, 285.6, and 290.3 eV, which correspond to C=N, C=C, C–C, C–N, and C=O, π-π* excitation, respectively. The peak area ratios of C=C double bonds and C–C single bonds of TFB-BZD_3-MDA_0-COF film is 2.33 while the TFB-BZD_2-MDA_1-COF, TFB-BZD_1-MDA_2-COF and TFB-BZD_0-MDA_3-COP film is 2.13, 1.94, 1.70, respectively (Figure S4a–d). The gradual decrease in the peak area ratios of C=C double bonds and C–C single bonds indicates a gradual increase in the proportion of C–C single bonds, which is mainly attributed to the increased MDA content introducing many methylenes with C–C single bonds. We also integrated the ^{13}C nuclear magnetic resonance (^{13}C NMR) of TFB-BZD_2-MDA_1-COF, TFB-BZB_1-MDA_2-COF and TFB-BZD_0-MDA_3-COP to further determine the composition of the films using the ratio method (Figure S3b–d). The peak area ratios at 41 and 157 ppm for TFB-BZD_2-MDA_1-COF, TFB-BZD_1-MDA_2-COF, and TFB-BZD_0-MDA_3-COP are 0.29, 0.63, and 0.87, respectively, which are similar to the MDA addition ratios of the three films. Combining the charge distribution maps of the two monomers, the ^{13}C NMR result and the XPS result, we concluded that MDA and BZD have similar reactivity. Due to structural differences in the four films, they also exhibit different microscopic morphologies (Figure S5 and Figure S6). With the increase of MDA monomer content, the apparent morphology of COF films changes from spherical packing to elongated packing. The incorporation of MDA may alter the symmetric structure of the COF, affecting its self-assembly results and producing different microstructures.

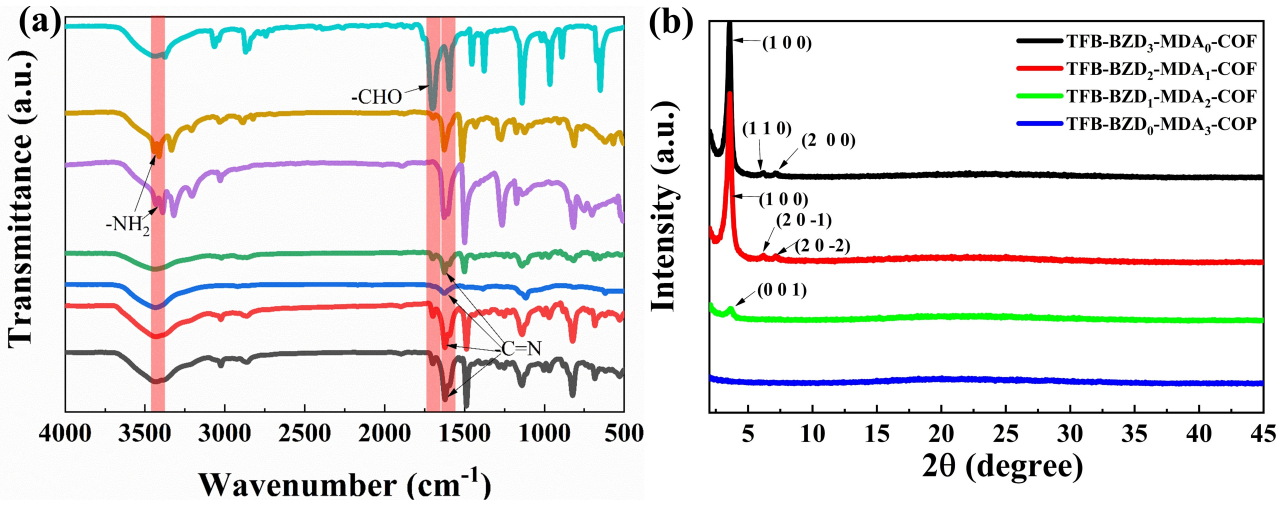

Figure 2. (a) Fourier transform infrared spectrometer of TFB-BZD_3-MDA_0-COF (black), TFB-BZD_2-MDA_1-COF (red), TFB-BZD_1-MDA_2-COF (blue), TFB-BZD_0-MDA_3-COP (green), BZD (purple), MDA (yellow) and TFB (cyan); (b) XRD patterns of the COF or COP films.

Similar phenomenon was also observed in other references.[22] Figure S5d and Figure S6d show that the irregular network structure of TFB-BZD_0-MDA_3-COP is due to unformed interlayer stacking. So, we think TFB-BZD_0-MDA_3-COP is a highly crosslinked covalent organic polymer rather than a two dimensional (2D) polymer like COF.

Nitrogen sorption isotherm measurements at 77 K were performed to investigate the porosity (Figure 3a–f and Figure S7). The specific surface areas of TFB-BZD_3-MDA_0-COF, TFB-BZD_2-MDA_1-COF, TFB-BZD_1-MDA_2-COF, TFB-BZD_0-MDA_3-COP are 929.7 m^2/g, 556.0 m^2/g, 104.5 m^2/g, 10.7 m^2/g, respectively. The corresponding pore capacities are 0.53 cm^3/g, 0.39 cm^3/g, 0.18 cm^3/g, 0.06 cm^3/g, respectively. As the MDA content increases, the specific surface area and pore capacity of the films decreases due to the decreased crystallinity. The pore size distributions of TFB-BZD_3-MDA_0-COF and TFB-BZD_2-MDA_1-COF are mainly concentrated within 5 nm and have a significant pore size distribution at 2.6 nm (which is consistent with the XRD results), while TFB-BZD_1-MDA_2-COF and TFB-BZD_0-MDA_3-COP also feature a larger pore size distribution (>5 nm). This result suggests the reduced crystallinity produces more non-crystalline regions in which the larger pores exist. In addition, all COF films have a wider range of pore sizes, which may be due to partial pore collapse during the preparation process and blockage of amorphous regions in the films.[22–23] TFB-BZD_0-MDA_3-COP exhibits a combination of adsorption and desorption curves due to its relatively low adsorption value.

To further determine the relative positions of BZD and MDA in the periodic structure of COF, we used the density functional tight binding (DFTB) method to calculate the interlayer interaction forces of three different structures of TFB-BZD_2-MDA_1-COF and TFB-BZD_1-MDA_2-COF, respectively, according to formula Eq. (1).

$$E_{\text{Interlayer interaction}} = E_2 - 2 \times E_1 \quad (1)$$

$E_{\text{Interlayer interaction}}$ is the interaction force between two layers of COF, E_2 is the total energy of the double-layer COF, and E_1 is the total energy of the single-layer COF. Table S1 shows the interlayer interactions of para-TFB-BZD_2-MDA_1-COF, ortho-TFB-BZD_2-MDA_1-COF, and meta-TFB-BZD_2-MDA_1-COF are 137.0, 136.8, 129.6 kcal/mol respectively while the interlayer interactions of para-TFB-BZD_1-MDA_2-COF, ortho-TFB-BZD_1-MDA_2-COF, and meta-TFB-BZD_1-MDA_2-COF are 137.9, 128.2,

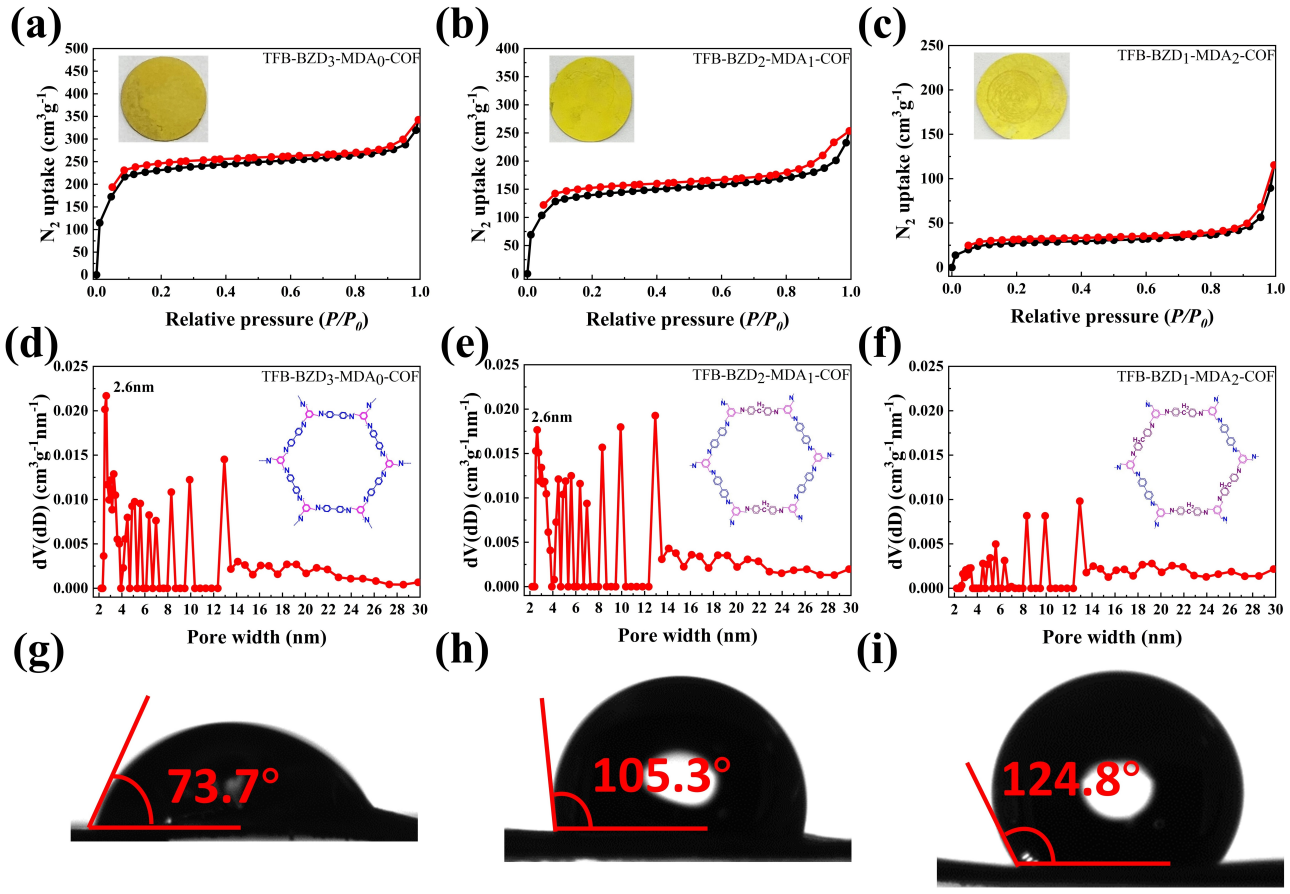

Figure 3. Nitrogen adsorption isotherm curves of films (a) TFB-BZD_3-MDA_0-COF, (b) TFB-BZD_2-MDA_1-COF and (c) TFB-BZD_1-MDA_2-COF; Pore size and pore size distribution profiles of films, (d) TFB-BZD_3-MDA_0-COF, (e) TFB-BZD_2-MDA_1-COF and (f) TFB-BZD_1-MDA_2-COF; Water contact angle of the film, (g) TFB-BZD_3-MDA_0-COF, (h) TFB-BZD_2-MDA_1-COF and (i) TFB-BZD_1-MDA_2-COF.

133.0 kcal/mol, respectively. According to the interlayer interaction force, para-TFB-BZD_2-MDA_1-COF and para-TFB-BZD_1-MDA_2-COF are easier to stack, which is more in line with the structural properties of COF periodic layered stacking.

The dielectric constant/loss of different COF or COP films were tested by a broadband dielectric analyzer (Figure 4). As the relative content of MDA increases in the frequency range of 10^2 to 10^6 Hz. The dielectric constant firstly shows a decreasing trend and then an increasing trend. Among them, TFB-BZD_3-MDA_0-COF reaches a dielectric constant of 2.2 (at 1 kHz), while TFB-BZD_2-MDA_1-COF yields the lowest dielectric constant of 1.9 (at 1 kHz), which decreases by 14 % compared to TFB-BZD_3-MDA_0-COF. The reasonable explanation is as follows: The methylene groups from MDA are flexible and cause the COF plane to become wavy, as shown in Figure 1. This distortion causes the spacing between layers to increase. In detail, the interlayer spacing of TFB-BZD_3-MDA_0-COF is 3.4 Å while it arrives at 3.8 Å for TFB-BZD_2-MDA_1-COF, therefore resulting in a decrease in interlayer electronic coupling and a decrease in the dielectric constant of the film.[15] Also, when MDA is introduced, it reduces the degree of conjugation of the material due to its non-planar nature,[24] which further reduces the electron migration distance under the electric field and therefore reduces the dielectric constant.[25] However, as the relative content of MDA further increases, we do not see an expected decrease in the dielectric constant (Figure S8). This is mainly because the continuously increased MDA content can cause the interlayer spacing of COF to give a rise (4.0 Å for TFB-BZD_1-MDA_2-COF), in return leading to a serious decrease in the crystallinity of the film (Figure 2b), as well as an obvious decrease in specific surface area and pore volume. The reduction of holes increases the polarization density, thus giving a rise to dielectric constant.[26] In comparison, the dielectric loss of the four thin films is inversely proportional to the relative content of MDA. From Figure 4b, TFB-BZD_3-MDA_0-COF has the highest dielectric loss (0.0038, at 1 kHz), mainly attributed to its high interlayer electron coupling and relatively low band gap (Figure 5a). Noticeably, the TFB-BZD_3-MDA_0-COF shows the highest conductivity (Figure 4c). As MDA content increases, the thin film's dielectric loss gradually decreases (Figure S8). At 1 kHz, the dielectric loss of TFB-BZD_2-MDA_1-COF and TFB-BZD_1-MDA_2-COF are 0.0029 and 0.0015, respectively. In comparison, the TFB-BZD_0-MDA_3-COP has a dielectric loss of 0.0012, which is lower than several pure polymers. For instance, Jiang reported a dielectric loss of around 0.01 for pure benzoxazole-polymer (PBO),[27] while Feng et al. reported a dielectric loss above 0.002 for pure polyimide (PI).[28] We also tested the dielectric constant of TFB-BZD_2-MDA_1-COF at high temperatures and 1 kHz (Figure S9). Films with an ultra-low dielectric constant (1.95) and ultra-low dielectric loss (0.0052) at 200 °C This is because TFB-BZD_2-MDA_1-COF is a highly cross-linked polymer and the

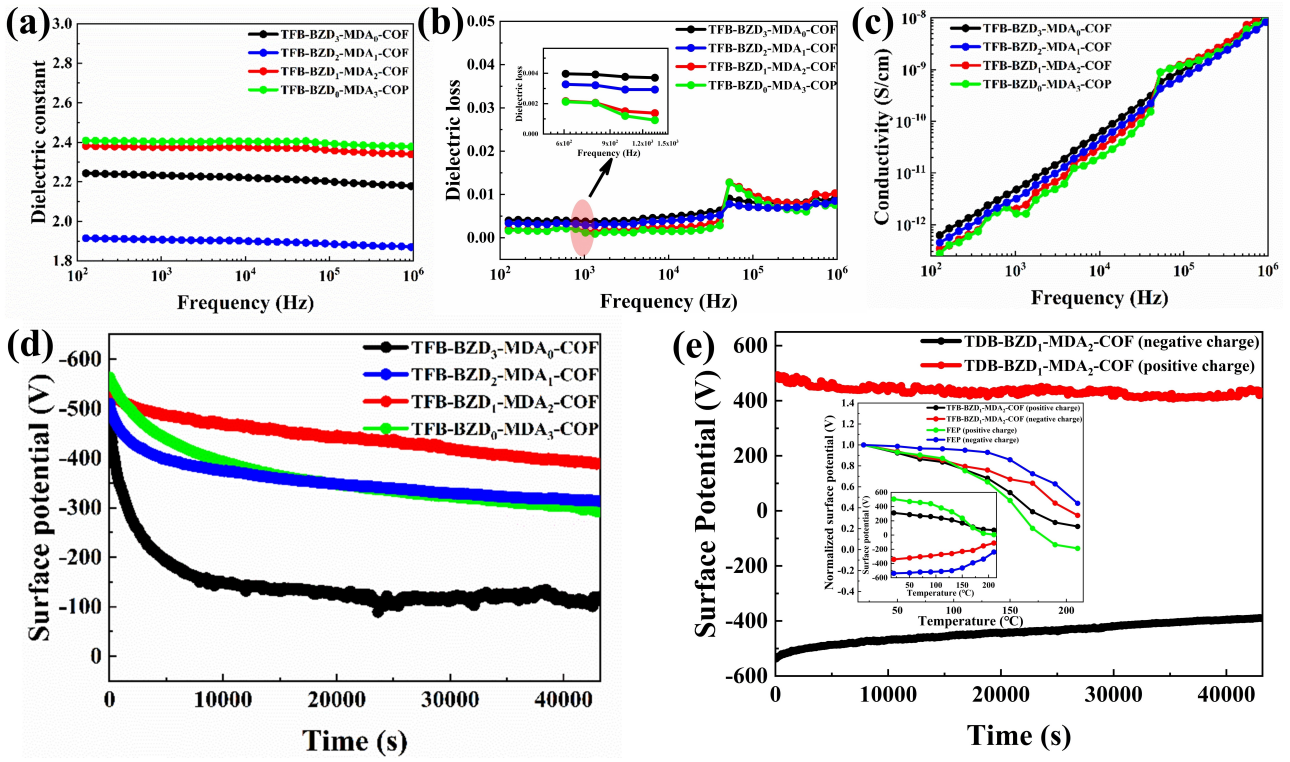

Figure 4. (a) Dielectric constant of films; (b) Dielectric loss of films; the inserted Figure showing the dielectric loss of films at 600–1500 Hz; (c) Conductivity of films; (d) The isothermal surface potential decay results of films at room temperature; (e) The isothermal surface potential decay results of TFB-BZD_1-MDA_2-COF at room temperature; the inserted figure showing the result of variable temperature versus normalized/unnormalized surface potential decay for TFB-BZD_1-MDA_2-COF.

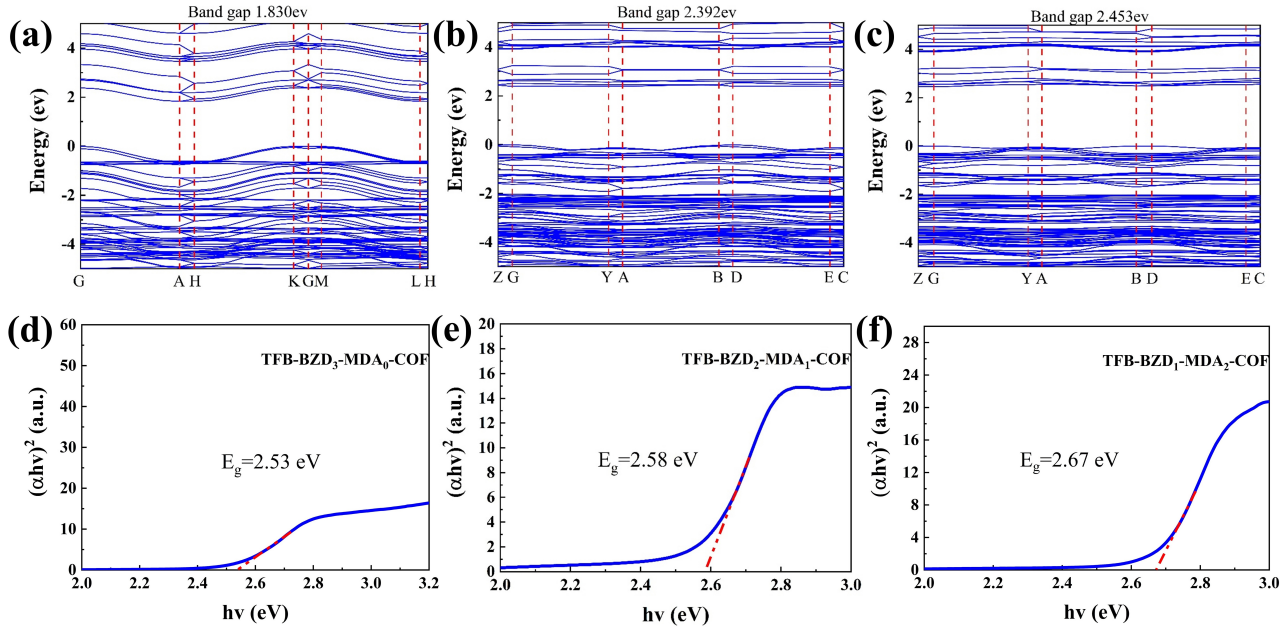

Figure 5. Band structure of (a) TFB-BZD_3-MDA_0-COF, (b) TFB-BZD_2-MDA_1-COF and (c) TFB-BZD_1-MDA_2-COF; Tauc plot analysis of COF thin films showing direct optical band gaps (d) TFB-BZD_3-MDA_0-COF, (e) TFB-BZD_2-MDA_1-COF and (f) TFB-BZD_1-MDA_2-COF.

cross-linked structure restricts the movement of the molecular chains, which results in an ultra-low dielectric constant and loss.[29] The dielectric properties of as-prepared COF are outstanding comparing to previous material systems that have been reported.[5b,30] (Figure S10).

Porous materials typically have a higher dielectric constant and dielectric loss in humid conditions due to the water-induced dielectric effect. To assess COF film quality, we measured the hydrophilicity of four thin films. As shown in Figure 3g–i and Figure S11, as the content of MDA increases, the contact angle increases from the initial 73.7° (TFB-BZD_3-MDA_0-COF) to 134.4° (TFB-BZD_0-MDA_3-COP), among which TFB-BZD_2-MDA_1-COF shows good hydrophobicity (105.3°). The reason for this is mostly due to the effective hydrophobicity resulting from the presence of methylene. Meanwhile, the hydrophobicity of the film is also enhanced as the amounts of methylene increases.

On the other hand, the backbone contains rigid chain segments and many pores due to the intrinsic cross-linked features. Therefore, the film has good thermal stability and a certain ability to store charge. As shown in Figure S12a-d, the 5 % weight loss temperature (T_{d5}) of TFB-BZD_3-MDA_0-COF, TFB-BZD_2-MDA_1-COF, TFB-BZD_1-MDA_2-COF, and TFB-BZD_0-MDA_3-COP in a nitrogen environment are 473 °C, 473 °C, 459 °C and 456 °C, respectively. With the increase of MDA content, T_{d5} shows a downward trend because methylene is more prone to fracture at high temperatures. In addition, we also conducted differential scanning calorimetry (DSC) tests on four types of films (Figure S13), and the DSC curves of all four films were relatively flat without obvious glass transition temperature (T_g) inflection points. This is because films featuring a high degree of crosslinking and crystallizing inhibit glass transition, which may result in higher processing temperatures. Similarly, due to the high degree of cross-linking of TFB-BZD_2-MDA_1-COF, its coefficient of thermal expansion is only 44 ppm/k (Figure S14). A lower coefficient of thermal expansion reduces stress in the film and copper sheet during high-temperature processing.

Some dielectrics can quasi-permanently store electric charges at their surface and/or in their bulk. Such dielectrics are defined as electrets. Electrets can exhibit various functionalities, including electrostatic, piezoelectric, pyroelectric, ferroelectric, biological, and nonlinear optical effects. As a result, they have gained significant attention from academia and industry.[18a] Studies have shown that the boundary between the air and matrix phases (pore walls) in the COF films created can retain charges and function as a charge trap, enabling the storage of a specific amount of charge. To the best of our knowledge, this is the first report on electric charge storage capacity based on the COF system. According to Figure 4d, the charge storage capacity of the films increases and then decreases with the increase of MDA content. The TFB-BZD_1-MDA_2-COF film exhibits the best charge storage capability and maintains a surface potential of around 320 V after one week, as shown in Figure S15. The increased MDA content leads to a higher band gap and lower conductivity, preventing surface potential decay. It appears that the surface potential of TFB-BZD_1-MDA_2-COF is higher than that of TFB-BZD_2-MDA_1-COF. This difference could be attributed to the numerous interfaces between crystalline and amorphous regions in the TFB-BZD_1-MDA_2-COF film, which may create an abundance of traps.[31] However, excessive MDA content will lead to fewer traps due to the relatively large pores and small specific surface of TFB-BZD_0-MDA_3-COP, which results in the reduction of charge trapping sites, therefore weakening the charge storage capacity. In addi-

tion, hydrophobicity is a key parameter of the electret as the charge storage capacity of the film is severely inhibited in humid environments because water neutralizes the charge stored in the polymer.[18c] With the increase of MDA content, the hydrophobicity of the film also rises thanks to the good hydrophobicity of methylene. TFB-BZD_1-MDA_2-COF has a water contact angle of 124.8° (Figure 3i), and the quite good hydrophobicity is an important reason why TFB-BZD_1-MDA_2-COF can retain charge well under normal environmental conditions. Compared to the most typical poly(4-fluorostyrene) (FPS) (97.3°) reported by Zhang et al., this resulting COF film has more excellent hydrophobicity.[18a]

As shown in Figure 4e, TFB-BZD_1-MDA_2-COF exhibits rather good thermal stability of the stored charge. When compared to the most advanced electret material on the market, called Perfluorinated ethylene-propylene copolymer (FEP), the film's negative electrical storage capacity weakens at high temperatures. This is mainly due to FEP containing a large amount of fluorine which plays a role in electron absorption. However, the film's positive electrical storage capacity is better than that of FEP at high temperatures (with a decay of surface potential of more than 50 % at 150 °C). Both the positive and negative surface potential of the film do not decay beyond 50 % at 150 °C. COF is a highly cross-linked crystalline polymer that can inhibit carrier migration with limited molecular chain motion at high temperatures..[32] Meanwhile, the negative electrical storage capacity of the film is better than the positive electrical storage capacity, which may be due to the presence of unreacted aldehyde groups in the film, which provide electron-absorbing capacity.

To discuss the relationship between dielectric constant, dielectric loss, charge storage, band gap, and structure more clearly, we further used the DFTB method to simulate the band structure of TFB-BZD_3-MDA_0-COF, TFB-BZD_2-MDA_1-COF, and TFB-BZD_1-MDA_2-COF (Due to the non-periodic structure of TFB-BZD_0-MDA_3-COP, band structure simulation is not performed on it), and the band gap ($E_g = E_{HOMO}$-E_{LUMO}, E_g is band gap; E_{HOMO} is highest occupied molecular orbital energy level; E_{LUMO} is lowest unoccupied molecular orbital energy level) of TFB-BZD_0-MDA_3-COP was calculated by DFT method. As shown in Figure 5a–c and Figure S21b, the E_g of TFB-BZD_3-MDA_0-COF is 1.83 eV, while the corresponding values for TFB-BZD_2-MDA_1-COF, TFB-BZD_1-MDA_2-COF, and TFB-BZD_0-MDA_3-COP are 2.392 eV, 2.453 eV, and 2.89 eV, respectively. With the increase of MDA content, the band gap of COF films increases, which is favorable for suppressing the intrinsic charge carriers. This also results in smaller dielectric loss and better charge storage performance of TFB-BZD_2-MDA_1-COF and TFB-BZD_1- MDA_2-COF films. At the same time, the TFB-BZD_3-MDA_0-COF has more significant band dispersion in the out-of-plane direction (Figure 5a), indicating that TFB-BZD_3-MDA_0-COF shows higher charge transport ability in the out of plane direction.[33] This is why the film possesses high conductivity and interlayer charge coupling, which leads to higher dielectric losses and poor charge storage capacity. To demonstrate the validity of our simulations, we conducted Ultraviolet diffuse reflection tests on four films to determine their band gap (Figure 5d-f and Figure S21b). All optical band gap energy trends (2.53–2.91 eV) of these COF or COP films are in good agreement with the theoretical band gap energy trends. As shown in Figure S22, the Ultraviolet absorption of TFB-BZD_1-MDA_2-COF shifts to a lower wavelength relative to TFB-BZD_3-MDA_0-COF and TFB-BZD_2-MDA_1-COF, which is the change in energy difference caused by the bending of the plane of COF.

As the complexity of integrated circuits increases, thermal conductivity is also another key index.[34] The current method to increase thermal conductivity is usually to add inorganic fillers with high thermal conductivity (such as boron nitride, graphene), but they have a high dielectric constant (above 4.5) and conductivity, which will increase the dielectric constant and dielectric loss of the material. We measured the thermal conductivity of four thin films (Table S2). The thermal conductivity of TFB-BZD_3-MDA_0-COF, TFB-BZD_2-MDA_1-COF, TFB-BZD_1-MDA_2-COF, and TFB-BZD_0-MDA_3-COP were 0.10, 0.12, 0.13, and 0.11 $Wm^{-1}K^{-1}$ (at room temperature), respectively. We have summarized the past relevant results in Table S3. Although the polyimide aerogel reported by Zha et al. has sensitive capacitive sensing and is well suited for electronics, the thermal conductivity of this aerogel is only 0.052 $Wm^{-1}K^{-1}$.[35] To solve the problem of low thermal conductivity of aerogels in electronics, Meador et al. prepared Polyamide Aerogels with high thermal conductivity, but the thermal conductivity of this aerogel (0.08 $Wm^{-1}K^{-1}$) is still lower than that of our COF film (0.12 $Wm^{-1}K^{-1}$).[36] Compared to other porous materials (thermal conductivity ranging from 0.02 to 0.05 $Wm^{-1}K^{-1}$),[36] TFB-BZD_2-MDA_1-COF and TFB-BZD_1-MDA_2-COF have higher thermal conductivity. Herein, as the MDA content gradually increases, the thermal conductivity first increases and then decreases. This is because for nanoporous materials, the pore size is comparable to the mean free path of phonons, and the air in the pores is unable to transfer heat by conduction. When the MDA content increases, the film's porosity decreases and the number of large pores increases (Figure 3d–f and Figure S7b), which facilitates the elevated thermal conductivity.[37] However, when the MDA content increases further, TFB-BZD_0-MDA_3-COP becomes an amorphous porous polymer, making it impossible for phonons to transfer energy through lattice vibrations, leading to a decrease in thermal conductivity.

Conclusion

In this paper, we thoroughly investigated the dielectric properties, charge storage capacity, and thermal properties of COF films by simply adjusting the MDA concentrations. The interlayer electronic coupling in COF films can be effectively suppressed by changing the curvature of the COF plane and increasing the gap between adjacent layers, thus reducing the dielectric constant (1.9 at 1 kHz) and dielectric loss (0.0029 at 1 kHz) for TFB-BZD_2-MDA_1-COF film.

High thermal decomposition temperature (T_{d5}, 473 °C) and good hydrophobicity (water contact angle, 105.3°) are also obtained in the resulting COF films. Also, to the best of our knowledge, our work is the first study reporting that the developed TFB-BZD_1-MDA_2-COF film can maintain high surface potential (≈320 V) within one week storage due to high porosity features, presenting great potentials in electret applications. Since COF is a periodic net structure, high-temperature dielectric properties are another highlighted point. The resulting TFB-BZD_2-MDA_1-COF presents an ultra-low dielectric constant (1.95) and ultra-low dielectric loss (0.0052) at 200 °C. Meanwhile, TFB-BZD_1-MDA_2-COF retains more than 50 % of its surface potential at 150 °C. In summary, the dielectric properties and charge storage capacity can be effectively adjusted by changing COF films' planar bending degree. Therefore, this innovative work lays a solid foundation for further research of COF derivates for smart electronic circuit material applications.

Supporting Information

The Supporting Information is available free of charge on the Wiley Publications website. Experimental procedures and characterization data, including Figure S1–S22 and Table S1–S3 (PDF).

Acknowledgements

All authors are grateful for financial support from the National Natural Science Foundation of China (52073091, 52303083, 52373073, 2171086), Shanghai Pujiang Program (22PJ1402500), Shanghai Rising-Star Program (21QA1403900) and the Key Laboratory of Advanced Polymer Materials of Shanghai.

Conflict of Interest

The authors declare no conflict of interest.

Data Availability Statement

The data that support the findings of this study are available from the corresponding author upon reasonable request.

Keywords: Charge Storage Capacity · Covalent Organic Framework Films · High Hydrophobicity · Ultra-Low Dielectric Constant

[1] a) X. Y. Huang, C. Y. Zhi, P. K. Jiang, D. Golberg, Y. Bando, T. Tanaka, *Adv. Funct. Mater.* **2013**, *23*, 1824–1831; b) X. Y. Feng, Y. Y. Lv, L. Zhang, J. J. Ding, J. Sun, X. X. Li, L. Chen, K. Zheng, X. Zhang, X. Y. Tian, *Adv. Eng. Mater.* **2020**, *22*, 1901486.

[2] W. F. Peng, H. Y. Lei, L. H. Qiu, F. Bao, M. J. Huang, *Polym. Chem.* **2022**, *13*, 3949–3955.

[3] a) D. Shamiryan, T. Abell, F. Iacopi, K. Maex, *Mater. Today* **2004**, *7*, 34–39; b) Y. D. Feng, K. Jin, J. Guo, C. C. Wang, *Polym. Chem.* **2021**, *12*, 4812–4821; c) Y. Zhang, Z. Y. Liu, X. L. Zhang, S. Y. Guo, *Ind. Eng. Chem. Res.* **2021**, *60*, 11749–11759; d) L. Wang, J. Yang, W. H. Cheng, J. J. Zou, D. Zhao, *Front. Mater.* **2021**, *8*, 774843; e) M. Krishtab, I. Stassen, T. Stassin, A. J. Cruz, O. O. Okudur, S. Armini, C. Wilson, S. De Gendt, R. Ameloot, *Nat. Commun.* **2019**, *10*, 3729.

[4] A. Borchers, T. Pieler, *Genes* **2010**, *1*, 413–426.

[5] a) H. W. Lee, Y. L. Liu, *J. Appl. Polym. Sci.* **2022**, *139*, 52605; b) K. Zhang, B. R. Hao, H. Ishida, *Polymer* **2021**, *223*, 123703; c) Y. D. Zhao, M. L. Yuan, L. T. Wang, X. Lu, Z. Xin, *Macromol. Mater. Eng.* **2022**, *307*, 2100747.

[6] K. Zhang, Q. X. Zhuang, Y. C. Zhou, X. Y. Liu, G. Yang, Z. W. Han, *J. Polym. Sci. Part A* **2012**, *50*, 5115–5123.

[7] J. Y. Qin, H. P. Zhao, Z. L. Qin, W. C. Zhang, R. J. Yang, *Polym. Compos.* **2021**, *42*, 3445–3457.

[8] Z. W. Zhang, D. Tian, Z. Q. Niu, Y. J. Zhou, X. Hou, X. Y. Ma, *Polym. Compos.* **2021**, *42*, 6900–6911.

[9] a) J. Y. Hu, F. Zanca, G. J. McManus, I. A. Riha, H. G. T. Nguyen, W. Shirley, C. G. Borcik, B. J. Wylie, M. Benamara, R. D. van Zee, P. Z. Moghadam, H. Beyzavi, *ACS Appl. Mater. Interfaces* **2021**, *13*, 21740–21747; b) C. Qian, Q. Y. Qi, G. F. Jiang, F. Z. Cui, Y. Tian, X. Zhao, *J. Am. Chem. Soc.* **2017**, *139*, 6736–6743; c) H. Xu, J. Gao, D. L. Jiang, *Nat. Chem.* **2015**, *7*, 905–912; d) Q. R. Fang, Z. B. Zhuang, S. Gu, R. B. Kaspar, J. Zheng, J. H. Wang, S. L. Qiu, Y. S. Yan, *Nat. Chem.* **2014**, *5*, 4503; e) S. Kandambeth, B. P. Biswal, H. D. Chaudhari, K. C. Rout, H. S. Kunjattu, S. Mitra, S. Karak, A. Das, R. Mukherjee, U. K. Kharul, R. Banerjee, *Adv. Mater.* **2017**, *29*, 1603945; f) S. Gao, Z. Y. Li, Y. Y. Yang, Z. Z. Wang, Y. L. Wang, S. J. Luo, K. S. Yao, J. K. Qiu, H. Y. Wang, L. Cao, Z. P. Lai, J. J. Wang, *ACS Appl. Mater. Interfaces* **2021**, *13*, 36507–36516.

[10] a) H. W. Fan, A. Mundstock, A. Feldhoff, A. Knebel, J. H. Gu, H. Meng, J. Caro, *J. Am. Chem. Soc.* **2018**, *140*, 10094–10098; b) S. Aydin, C. Altintas, S. Keskin, *ACS Appl. Mater. Interfaces* **2022**, *14*, 21738–21749.

[11] a) Y. Y. He, N. An, C. C. Meng, L. Z. K. Xiao, Q. Q. Wei, Y. Zhou, Y. Y. Yang, Z. M. Li, Z. G. Hu, *ACS Appl. Mater. Interfaces* **2022**, *14*, 57328–57339; b) Y. Y. He, N. An, C. C. Meng, K. F. Xie, X. T. Wang, X. Y. Dong, D. M. Sun, Y. Y. Yang, Z. A. Hu, *J. Mater. Chem. A* **2022**, *10*, 11030–11038; c) S. Y. Wang, H. Fu, J. M. Ma, X. M. Shi, H. M. Wang, Z. Y. Yin, S. Zhang, M. D. Jin, Z. Y. Zhong, X. Y. Zhai, Y. P. Du, *Chem. Sci.* **2022**, *13*, 12367–12373; d) E. Vitaku, C. N. Gannett, K. L. Carpenter, L. Shen, H. D. Abruña, W. R. Dichtel, *J. Am. Chem. Soc.* **2020**, *142*, 16–20.

[12] a) R. S. B. Gonçalves, A. B. V. De Oliveira, H. C. Sindra, B. S. Archanjo, M. E. Mendoza, L. S. A. Carneiro, C. D. Buarque, P. M. Esteves, *ChemCatChem* **2016**, *8*, 743–750; b) Y. J. Chen, H. Y. Zhuo, Y. Pan, J. X. Liang, C. G. Liu, J. Li, *Sci. China Mater.* **2021**, *64*, 1939–1951; c) S. Q. Gao, Q. Zhang, X. F. Su, X. K. Wu, X. G. Zhang, Y. Y. Guo, Z. Y. Li, J. S. Wei, H. Y. Wang, S. J. Zhang, J. J. Wang, *J. Am. Chem. Soc.* **2023**, *145*, 9520–9529.

[13] a) L. Wang, H. J. Xie, Y. X. Lin, M. H. Wang, L. J. Sha, X. M. Yu, J. Yang, J. Zhao, G. X. Li, *Biosensors Bioelectronics* **2022**, *217*, 114668; b) Y. K. Yang, H. H. Wei, X. M. Wang, D. D. Sun, L. G. Yu, B. Q. Bai, X. Jing, S. Qin, H. L. Qian, *Biosensors Bioelectronics* **2023**, *223*, 115017; c) M. Liu, Y. J. Chen, X. Huang, L. Z. Dong, M. Lu, C. Guo, D. Q. Yuan, Y. F. Chen, G. Xu, S. L. Li, Y. Q. Lan, *Angew. Chem. Int. Ed.* **2022**, *61*, 202115308; d) S. Bag, H. S. Sasmal, S. P. Chaudhary, K. Dey, D. Blätte, R. Guntermann, Y. Y. Zhang, M. Položij, A. Kuc,

A. Shelke, R. K. Vijayaraghavan, T. G. Ajithkumar, S. Bhattacharyya, T. Heine, T. Bein, R. Banerjee, *J. Am. Chem. Soc.* **2023**, *145*, 1649–1659.

[14] a) J. R. Zhen, S. Y. Ding, W. Wang, J. M. Liu, J. L. Sun, Z. T. Huang, Q. Y. Zheng, *Chin. J. Chem.* **2016**, *34*, 783–787; b) M. C. Wang, M. Wang, H. H. Lin, M. Ballabio, H. X. Zhong, M. Bonn, S. Q. Zhou, T. Heine, E. Canovas, R. H. Dong, X. L. Feng, *J. Am. Chem. Soc.* **2020**, *142*, 21622–21627; c) T. T. Feng, D. Streater, B. Sun, K. Duisenova, D. Wang, Y. Liu, J. E. Huang, J. Zhang, *J. Phys. Chem. Lett.* **2022**, *13*, 1398–1405; d) K. R. Cai, W. J. Wang, J. Zhang, L. Chen, L. K. Wang, X. J. Zhu, Z. P. Yu, Z. C. Wu, H. P. Zhou, *J. Mater. Chem. A* **2022**, *10*, 7165–7172; e) H. V. Babu, M. G. M. Bai, M. R. Rao, *ACS Appl. Mater. Interfaces* **2019**, *11*, 11029–11060.

[15] P. P. Shao, J. Li, F. Chen, L. Ma, Q. B. Li, M. X. Zhang, J. W. Zhou, A. X. Yin, X. Feng, B. Wang, *Angew. Chem. Int. Ed.* **2018**, *57*, 16501–16505.

[16] A. M. Evans, A. Giri, V. K. Sangwan, S. N. Xun, M. Bartnof, C. G. Torres Castanedo, H. B. Balch, M. S. Rahn, N. P. Bradshaw, E. Vitaku, D. W. Burke, H. Li, M. J. Bedzyk, F. Wang, J. L. Brédas, J. A. Malen, A. J. H. McGaughey, M. C. Hersam, W. R. Dichtel, P. E. Hopkins, *Nat. Mater.* **2021**, *20*, 1142.

[17] S. Kandambeth, K. Dey, R. Banerjee, *J. Am. Chem. Soc.* **2019**, *141*, 1807–1822.

[18] a) Y. W. Zhu, Y. K. Fan, S. T. Li, P. Wei, D. F. Li, B. Liu, D. M. Cui, Z. C. Zhang, G. C. Li, Y. J. Nie, G. H. Lu, *Mater. Horiz.* **2020**, *7*, 1861–1871; b) X. W. Mo, H. Zhou, W. B. Li, Z. S. Xu, J. J. Duan, L. Huang, B. Hu, J. Zhou, *Nano Energy* **2019**, *65*, 104033; c) H. Y. Li, Z. H. Guo, S. Y. Kuang, H. L. Wang, Y. Wang, T. Wu, Z. L. Wang, G. Zhu, *Nano Energy* **2019**, *64*, 103913.

[19] W. P. Li, W. Xie, F. Shao, J. Qian, S. T. Han, P. Wen, J. Lin, M. Chen, X. R. Lin, *Chem* **2023**, *9*, 117–129.

[20] J. T. Liu, G. Han, D. L. Zhao, K. J. Lu, J. Gao, T. S. Chung, *Sci. Adv.* **2020**, *6*, 1110.

[21] S. Y. Ding, J. Gao, Q. Wang, Y. Zhang, W. G. Song, C. Y. Su, W. Wang, *J. Am. Chem. Soc.* **2011**, *133*, 19816–19822.

[22] J. Ning, Y. Gao, X. D. Cao, H. T. Wei, B. Wang, L. Hao, *J. Energy Chem.* **2022**, *65*, 490–496.

[23] X. Tang, Q. Q. Zhang, D. Y. Chen, L. F. Deng, Y. X. He, J. X. Wang, C. Y. Pan, J. T. Tang, G. P. Yu, *Chem. Commun.* **2023**, *59*, 8731–8734.

[24] Z. Y. Ran, R. Wang, J. Fu, M. C. Yang, M. X. Li, J. Hu, J. L. He, Q. Li, *Adv. Mater.* **2023**, *2023*, 2303849.

[25] J. H. Song, H. M. Qin, S. Y. Qin, M. Liu, S. X. Zhang, J. Y. Chen, Y. Zhang, S. Wang, Q. Li, L. J. Dong, C. X. Xiong, *Mater. Horiz.* **2023**, *10*, 2139–2148.

[26] X. D. Dong, B. Q. Wan, M. S. Zheng, L. B. Huang, Y. Feng, R. F. Yao, J. H. Gao, Q. L. Zhao, J. W. Zha, *Adv. Mater.* **2023**, 2307804.

[27] J. H. Jiang, J. P. Li, J. Qian, X. Y. Liu, P. Y. Zuo, Y. Yuan, Q. X. Zhuang, *J. Mater. Chem. A* **2021**, *9*, 26010–26018.

[28] Q. K. Feng, Q. Dong, D. L. Zhang, J. Y. Pei, Z. M. Dang, *Compos. Sci. Technol.* **2022**, *218*, 109193.

[29] F. Le Goupil, V. Salvado, V. Rothan, T. Vidil, G. Fleury, H. Cramail, E. Grau, *J. Am. Chem. Soc.* **2023**, *145*, 4583–4588.

[30] a) C. Liu, M. Mullins, S. Hawkins, M. Kotaki, H. J. Sue, *ACS Appl. Mater. Interfaces* **2018**, *10*, 1250–1257; b) J. J. Wang, J. Sun, J. F. Zhou, K. K. Jin, Q. Fang, *ACS Appl. Mater. Interfaces* **2017**, *9*, 12782–12790; c) Z. Zhang, P. He, W. J. Ma, P. Y. Zuo, X. Y. Liu, Q. X. Zhuang, *Adv. Funct. Mater.* **2023**, *33*, 2302212; d) J. Wang, D. L. Zhou, X. Lin, J. H. Li, D. Han, H. W. Bai, Q. Fu, *Chem. Eng. J.* **2022**, *439*, 135737; e) Z. W. Zhang, Y. J. Zhou, L. F. Cai, L. X. Xuan, X. Wu, X. Y. Ma, *Chem. Eng. J.* **2022**, *439*, 135740; f) Z. D. Hu, Y. M. Wang, X. Q. Liu, Q. Wang, X. Cui, S. X. Jin, B. Yang, Y. M. Xia, S. H. Huang, Z. Qiang, K. Fu, J. M. Zhang, Y. W. Chen, *Compos. Sci. Technol.* **2022**, *223*, 109403; g) S. H. Han, Y. N. Li, F. Y. Hao, H. Zhou, S. L. Qi, G. F. Tian, D. Z. Wu, *Eur. Polym. J.* **2021**, *143*, 110206; h) J. M. Hao, Y. F. Wei, X. S. Li, J. X. Mu, *J. Appl. Polym. Sci.* **2018**, *135*, 46084; i) X. D. Li, J. C. Feng, S. Zhang, Y. Tang, X. Y. Hu, X. P. Liu, X. Q. Liu, *J. Appl. Polym. Sci.* **2021**, *138*, 49887; j) X. L. Zhang, M. Liu, Y. Chen, J. C. He, X. L. Wang, J. Xie, Z. W. Li, Z. M. Chen, Y. H. Fu, C. X. Xiong, S. Wang, *J. Appl. Polym. Sci.* **2022**, *139*, 52787; k) J. Lu, Y. Zhang, J. Li, M. F. Fu, G. X. Zou, S. J. Ando, Y. B. Zhuang, *Macromolecules* **2023**, *56*, 2164–2174.

[31] a) H. J. Hwang, H. M. Hong, B. G. Cho, H. K. Lee, J. S. Kim, U. J. Lee, W. Kim, H. Kim, K. B. Chung, D. Choi, *Nano Energy* **2021**, *90*, 106647; b) T. S. Sherkar, C. Momblona, L. Gil Escrig, J. Avila, M. Sessolo, H. J. Bolink, L. J. A. Koster, *ACS Energy Lett.* **2017**, *2*, 1214–1222.

[32] a) M. X. Yuan, G. Zhang, B. Li, T. C. M. Chung, R. Rajagopalan, M. T. Lanagan, *ACS Appl. Mater. Interfaces* **2020**, *12*, 14154–14164; b) J. L. Mao, S. Wang, L. Zhang, Y. Chen, Y. H. Cheng, *Int. J. Energy Res.* **2020**, *44*, 7580–7590.

[33] Y. H. Zhu, P. P. Shao, L. Y. Hu, C. Sun, J. Li, X. Feng, B. Wang, *J. Am. Chem. Soc.* **2021**, *143*, 7897–7902.

[34] F. L. Tan, S. Han, D. L. Peng, H. L. Wang, J. Yang, P. Zhao, X. J. Ye, X. Dong, Y. Y. Zheng, N. Zheng, L. Gong, C. L. Liang, N. Frese, A. Golzhauser, H. Qi, S. S. Chen, W. Liu, Z. K. Zheng, *J. Am. Chem. Soc.* **2021**, *143*, 3927–3933.

[35] X. D. Dong, B. Q. Wan, M. S. Zheng, X. Yang, H. K. Zhang, Q. L. Zhao, J. W. Zha, *Chem. Eng. J.* **2023**, *465*, 143034.

[36] J. C. Williams, B. N. Nguyen, L. McCorkle, D. Scheiman, J. S. Griffin, S. A. Steiner, M. A. B. Meador, *ACS Appl. Mater. Interfaces* **2017**, *9*, 1801–1809.

[37] G. H. Tang, C. Bi, Y. Zhao, W. Q. Tao, *Energy* **2015**, *90*, 701–721.

Manuscript received: October 8, 2023
Accepted manuscript online: November 14, 2023
Version of record online: November 22, 2023